



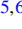



Two transitions in complex eigenvalue statistics: Hermiticity and integrability breaking

Gernot Akemann ^{1,2,*} Federico Balducci ^{3,4} Aurélia Chenu ^{3,†} Patricia Päßler ¹
 Federico Roccati ^{5,6} and Ruth Shir ^{3,‡}

¹Faculty of Physics, *Bielefeld University*, Postfach 100131, 33501 Bielefeld, Germany

²School of Mathematics, *University of Bristol*, Fry Building, Woodland Road, Bristol BS8 1UG, United Kingdom

³Department of Physics and Materials Science, *University of Luxembourg*, L-1511 Luxembourg

⁴Max Planck Institute for the Physics of Complex Systems, Nöthnitzer Strasse 38, 01187 Dresden, Germany

⁵Department of Physics, *Columbia University*, New York, New York 10027, USA

⁶Max Planck Institute for the Science of Light, Staudtstraße 2, 91058 Erlangen, Germany



(Received 15 October 2024; accepted 3 January 2025; published 27 January 2025)

Open quantum systems have complex energy eigenvalues which are expected to follow non-Hermitian random matrix statistics, when chaotic, or two-dimensional (2d) Poisson statistics, when integrable. We investigate the spectral properties of a many-body quantum spin chain, i.e., the Hermitian XXZ Heisenberg model with imaginary disorder. Its rich complex eigenvalue statistics is found to separately break both Hermiticity and integrability at different scales of the disorder strength. With no disorder, the system is integrable and Hermitian, with spectral statistics corresponding to the 1d Poisson point process. At very small disorder, we find a transition from 1d Poisson statistics to an effective D -dimensional Poisson point process, showing Hermiticity breaking. At intermediate disorder, we find integrability breaking, as inferred from the statistics matching that of non-Hermitian complex symmetric random matrices in class AI^\dagger . For large disorder, as the spins align, we recover the expected integrability (now in the non-Hermitian setup), indicated by 2d Poisson statistics. These conclusions are based on fitting the spin-chain data of numerically generated nearest- and next-to-nearest-neighbor spacing distributions to an effective 2d Coulomb gas description at inverse temperature β . We confirm that such an effective description of random matrices also applies in classes AI^\dagger and AII^\dagger up to next-to-nearest-neighbor spacings.

DOI: [10.1103/PhysRevResearch.7.013098](https://doi.org/10.1103/PhysRevResearch.7.013098)

I. INTRODUCTION

One of the most studied indicators of quantum chaos in isolated systems is the spectral statistics of nearest-neighbor eigenvalues. The quantum chaos conjectures by Berry and Tabor (BT) [1] and by Bohigas, Giannoni, and Schmit (BGS) [2] (cf. [3]) identify the nearest-neighbor spectral statistics as a tool to distinguish generic closed quantum chaotic systems from integrable ones. BT conjectured that generic closed quantum integrable systems have spectral statistics corresponding to the statistics of a Poisson point process in one dimension (1d Poisson). BGS conjectured that closed quantum chaotic systems follow spectral statistics of random matrices and are classified according to their symmetry classes. These conjectures were shown to work in many closed quantum systems [4] and the BGS conjecture was derived from a semiclassical expansion [5] (cf. [6]). The crossover

between chaos and integrability, where an integrability breaking term is added to an otherwise integrable model or an integrability restoring term is added to a chaotic model, was also studied [4,7].

Quantum systems are, in general, not perfectly isolated, but rather interact with their surrounding environment. When the timescales of the environment are much shorter than the system's timescales and under the Born approximation, the reduced system's dynamics can be effectively described by a Schrödinger equation with a non-Hermitian Hamiltonian [8–10] and thus generically has a complex spectrum. Grobe, Haake, and Sommers (GHS) [11] conjectured that for Markovian, open quantum systems, spectral properties can be used to distinguish between chaos and integrability, in a way similar to the Hermitian case. In particular, open quantum systems that are chaotic should display non-Hermitian random matrix statistics, while integrable systems with complex spectra should follow the statistics of a Poisson point process in two dimensions (2d Poisson). This conjecture was tested early on for the discrete quantum map of periodically kicked tops with damping [11] and in random neural networks [12]; see below for further recent examples. In both cases, the nearest-neighbor spacing distribution was found to agree with the 2d Poisson statistics in the integrable case, and with that of the complex Ginibre ensemble [13] in the fully chaotic regime.

Recently, the question of which symmetry class of random matrices is appropriate for dissipative systems has been

*Contact author: akemann@physik.uni-bielefeld.de

†Contact author: aurelia.chenu@uni.lu

‡Contact author: ruth.shir@uni.lu

reopened and explored in greater detail [14], revisiting the previously suggested Bernard-LeClair classification [15,16]. Based on numerical simulations, it was suggested that only three different symmetry classes of local bulk statistics exist [14], with representatives being classes A (complex Ginibre) [13], AI^\dagger (complex symmetric), and AII^\dagger (complex self-dual). Several authors have provided further examples for the non-Hermitian quantum chaos conjecture of GHS, finding a crossover from 2d Poisson to one of these random matrix statistics in quantum systems. These include examples from 2d random Schrödinger operators [17], 4d lattice quantum field theory with chemical potential [18,19], directed complex networks [20], quantum spin chains [14,21,22], kicked rotors [23], 2d Anderson models with disorder [24], and beyond physics in theoretical ecology [25].

The crossover between integrable and chaotic systems thus has currently been studied in systems that are either Hermitian—corresponding to going from a 1d Poisson process to a Hermitian random matrix ensemble—or non-Hermitian—corresponding to the transition going from a 2d Poisson to one of the non-Hermitian symmetry classes. However, the interplay between Hermiticity breaking and integrability breaking has never been investigated. We do it here by studying a strongly interacting many-body system with dissipative local disorder. In the absence of dissipation, disordered interacting quantum models have been the focus of much attention recently due to the presence of many-body localized phases [26–33]. These are robust, nonergodic phases of quantum matter that violate the eigenstate thermalization hypothesis [34,35] and display an emergent integrability via local integrals of motion [36–38]. Similar nonchaotic regimes have been conjectured to also be present in an open setting, especially in the context of non-Hermitian Hamiltonians [39–43].

The model considered in this work, introduced in Ref. [44], has the peculiarity of a purely imaginary disorder, breaking, at the same time, both integrability and Hermiticity. This model is motivated by a recent experimental work [45], showing that local tunable loss terms can be engineered in synthetic lattices. Moreover, the model allows us to investigate whether the breaking of Hermiticity happens on a different scale than the transition between chaotic and integrable behavior. We quantitatively characterize the crossovers by comparing the nearest-neighbor (NN) level statistics of complex eigenvalues to that of a static Coulomb gas in 2d. In order to go beyond the smallest local scale, we will also use next-to-nearest-neighbor (NNN) spacing distributions. The 2d Coulomb gas (2dCG) allows us to reproduce the 2d Poisson statistics and approximate the random matrix class AI^\dagger as a function of the Coulomb gas inverse temperature β [46], thus enabling one to capture a transition from integrable ($\beta = 0$) to chaotic ($\beta = 1.4$) behavior, respectively. The breaking of Hermiticity is captured through a D -dimensional Poisson point process, with D transitioning from a value of 1 for a purely Hermitian spectrum to 2 for strongly non-Hermitian systems.

The article is organized as follows. Section II describes our model, the XXZ spin chain with purely imaginary disorder, which is Hermitian and integrable at vanishing disorder, and its symmetries. The main Sec. III contains our results, namely, the transition between random matrix and 2d Poisson statistics in β of the 2dCG, and, for very small disorder,

the transition from 1d to 2d Poisson statistics, indicating a Hermiticity breaking crossover. In Sec. IV, we introduce the corresponding complex eigenvalue statistics for NN and NNN spacing distributions used to characterize the model, namely, first, an interpolating 2dCG ensemble for which an accurate surmise exists close to 2d Poisson statistics, second, Poisson point process statistics (in varying dimension D), and third, the random matrix statistics of class AI^\dagger , appropriate for the considered model. Section V describes our methods, in particular the unfolding procedure used in 2d and the tools to measure distances between two probability distributions. For completeness, we briefly present complex spacing ratios introduced by [47] as an alternative tool. Our conclusions and open questions are presented in Sec. VI. The Appendix summarizes the other two distinct random matrix symmetry classes A and AII^\dagger , including NN and NNN spacings.

II. XXZ MODEL WITH DISSIPATIVE DISORDER

This section describes the dissipative model that we consider, together with some aspects of its symmetries and spectrum.

A. Definition of the model

We consider a chain of L interacting spins with local dissipative disorder, described by the non-Hermitian Hamiltonian,

$$H = H_{\text{XXZ}} - i\Gamma/2, \quad (1)$$

with the XXZ spin-chain Hamiltonian,

$$H_{\text{XXZ}} = \sum_{a=1}^L (S_a^x S_{a+1}^x + S_a^y S_{a+1}^y + \Delta S_a^z S_{a+1}^z), \quad (2)$$

and

$$\Gamma = \sum_{a=1}^L \gamma_a \left(S_a^z + \frac{1}{2} \mathbb{1} \right) \quad (3)$$

representing site-dependent, local, *dissipative* disorder because of the imaginary i in (1). The site-dependent losses γ_a can be experimentally implemented, as demonstrated in a synthetic lattice [45]. Here, they are sampled from a uniform distribution $\mathcal{U}(0, \gamma)$, where γ represents the “strength” of the disorder. For each value of γ , we generate spectral data from a number of realizations of the model, each realization having a different randomly chosen set of local disorder terms, $\{\gamma_a\}_{a=1}^L$. We consider the case of periodic boundary conditions, as depicted in Fig. 1.

Note that in this model, all the disorder and its implications to the spectral statistics come from the openness of the system—the spin-chain Hamiltonian (2) is always fixed and is integrable according to the Bethe ansatz [48]. For the study of spectral statistics of non-Hermitian models with real disorder, see, e.g., [24,39,44]. In [44], it was shown that by increasing the range γ , the statistics of the *singular values* exhibit a crossover from chaotic to integrable. A similar observation is made here from the eigenvalue spacing statistics. We complete the story by extending the analysis to very small disorder, which reveals a richer behavior coming from Hermiticity breaking. For some aspects of thermalization and transport in

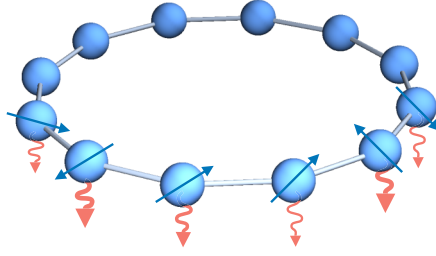


FIG. 1. Schematic illustration of the spin-chain model with local dissipative disorder described by Eq. (1).

this model, see [49]. This model preserves the total spin in the z direction, $S_z = \sum_{a=1}^L S_a^z$. We thus work in a specific total S_z magnetization sector, usually the largest one with $S_z = 0$ which occurs for even L and is of dimension $\binom{L}{L/2}$. Without disorder ($\gamma = 0$), additional symmetries need to be taken into account to avoid exact degeneracies in the spectrum (see, e.g., [50]). Specifically, each S_z sector then splits into two: one sector with states of even parity and another with states of odd parity.

The Hamiltonian (1) falls into the universality class AI^\dagger of non-Hermitian random matrices [14]. These are complex symmetric matrices which satisfy $H = H^T$, with $H \neq H^\dagger$. In addition, the non-Hermitian Hamiltonian (1) is pseudo-Hermitian, as shown in Sec. II B, and thus its complex eigenvalue spectrum is symmetric across a line parallel to the real axis of the complex plane at $(-i/4) \sum_{a=1}^L \gamma_a$.

B. Pseudo-Hermitian complex spectrum

The complex spectrum of the Hamiltonian (1) has reflection symmetry along a line parallel to the real axis, i.e., the eigenvalues come in complex conjugate pairs above and below this line. This reflection symmetry in the complex spectrum is a result of the matrix being *pseudo-Hermitian* [51–53]. A matrix is pseudo-Hermitian if there exists an invertible matrix S such that

$$H = SH^\dagger S^{-1}. \quad (4)$$

Indeed, if such a similarity transformation exists, and λ is an eigenvalue of H with right eigenvector $|R\rangle$, $H|R\rangle = \lambda|R\rangle$, then also λ^* is an eigenvalue of H . This can be shown by taking the Hermitian conjugate $H^\dagger|R^*\rangle = \lambda^*|R^*\rangle$ and using (4), giving $HS|R^*\rangle = \lambda^*S|R^*\rangle$, which means that λ^* is an eigenvalue of H with eigenvector $S|R^*\rangle$.

In our case, such an S would need to flip the sign of Γ in Eq. (3) [54], while keeping H_{XXZ} unchanged. It turns out that this can be achieved by the operator

$$S = \prod_{a=1}^L S_a^x, \quad (5)$$

which acts as $SS_a^x S^{-1} = +S_a^x$, $SS_a^y S^{-1} = -S_a^y$ and $SS_a^z S^{-1} = -S_a^z$ for any site a . In H_{XXZ} , the spin operators appear in pairs and so the sign change is canceled. In turn, the S_a^z operators appear once in each term of Γ , leading to $S\Gamma S^{-1} = -\Gamma$, as needed to fulfill the symmetry (4).

III. RESULTS FOR THE SPIN CHAIN

We now characterize the spectral statistics of the spin chain with dissipative disorder described by the non-Hermitian Hamiltonian (1). We do so by comparing the distributions of its eigenvalue spacings with that of the 2d spectral statistics of the reference models, detailed in Sec. IV, using the methods presented in Sec. V. We focus on the NN and NNN spacing distributions for values of the disorder strength in the range $\gamma = 0$ –20, fitting the numerical distribution to either the 2dCG distributions and finding the corresponding β or to a D -dimensional Poisson point process with $1 \leq D \leq 2$. For $L = 16$, we present NN, NNN, and complex spacing ratio data for over 450 disorder realizations, while for $L = 12, 14$, we show this data for 1000 disorder realizations. To complete the picture, a qualitative discussion of the complex spacing ratios [47] is included at the end of the section.

We expect the spectral statistics of our model to behave similarly to those of a XXZ spin-chain Hamiltonian with real disorder, which exhibits a crossover of the spectral statistics from chaos to integrability (for nonzero disorder strength) as the disorder strength is increased. In such a case, the NN spectral statistics changes from random matrix statistics approximated by the Wigner surmise $\propto se^{-as^2}$ for the Gaussian orthogonal ensemble (GOE) in this model to 1d Poisson statistics, $\propto e^{-s}$, with s standing for the spacing between NN eigenenergies. In 1d, there is universal level repulsion between the eigenvalues only in the first, chaotic regime, while in the second, 1d Poisson statistics displays uncorrelated eigenvalues—a universal signature of generic integrable (deterministic) systems.

In the non-Hermitian (2d) case with imaginary disorder, where the eigenvalues lie in the complex plane, we expect the spectral statistics to exhibit a crossover between random matrix statistics of class AI^\dagger in our case to that of the 2d Poisson point process—which has a linear repulsion from the area measure; see (9) at $D = 2$. We follow the proposal [21] and use the spectral statistics of a 2d Coulomb gas with some value for $\beta \geq 0$, which includes 2d Poisson statistics at $\beta = 0$ as a special case and approximates the AI^\dagger class for $\beta \approx 1.3$ –1.4 [46]. Fitting β thus allows us to capture this crossover. However, the transition has more structure than initially expected, showing two different crossovers, as we summarize below and detail in subsequent sections.

On a technical level, the spin-chain data need to be drawn away from the edges of the eigenvalue distributions, where the statistics may be different or not even universal, as discussed at the beginning of Sec. IV. To do so, we focus on the bulk given by the denser inner part of the spectrum. We systematically select only that part of the spectrum for which the eigenvalue density is not less than some fraction of the maximal density. For $L = 16$ spins with $\gamma = 0.75$ –20, we use 1/2 of the maximal density; for $L = 14$ and $L = 12$, we use 1/3 of the maximal density as a cutoff for the eigenvalues to be included in the analysis. For $L = 16$ spins with $\gamma < 0.75$, we choose a cutoff equal to or smaller than 1/4 the maximal density because, as we discuss below, the spectrum is very peaked around a line parallel to the real line.

The 2d spectral statistics of the D -dimensional Poisson process and 2dCG, detailed in Sec. IV, are presented in Fig. 2. For our analysis, the relevant features are as follows. The NN

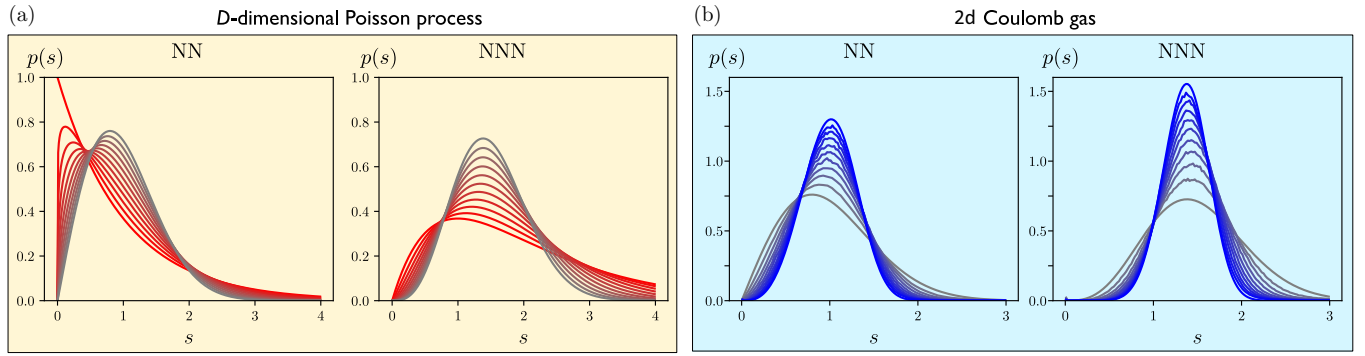


FIG. 2. (a) Spacing distributions of the NN and NNN for the Poisson process, with dimension $1 \leq D \leq 2$ varying in steps of 0.1 (red to gray). Notice that in both cases, the maximum moves from right to left when decreasing dimension D . (b) The numerically generated NN and NNN spacing distributions of the 2dCG for $\beta = 0-2$, increasing in steps of 0.2 (gray to blue). This also includes analytic formulas for 2d Poisson statistics with $\beta = 0$, (9) and (10) with the lowest maxima, and random matrix class A with $\beta = 2$, (A2), and (A3), with highest maxima. Note that the gray curves for $D = 2$ in (a) are the same as the gray curves for $\beta = 0$ in (b) since the two processes then coincide.

distribution of the 2dCG has its leftmost and lowest maximum at $\beta = 0$; see Fig. 2(b), left (gray curve). Increasing β leads to a monotonous increase of the maximum in height and in position to the right (gray to blue). The random matrix class AI^\dagger expected at maximal chaos is the one with the lowest maximum of the three distinct random matrix classes (see Fig. 13), reached at approximately $\beta \approx 1.3-1.4$. As such, it is approached by the 2dCG monotonously from below, starting at $\beta = 0$. What happens if the maximum of the NN spacing distribution of our spin-chain data—which is normalized and has first moment of unity—is to the *left* of the 2d Poisson distribution (at $\beta = 0$)? Obviously, the 2dCG will no longer provide a good fit. Only the D -dimensional Poisson distribution might provide a good fit for $D < 2$; see Fig. 2(a), left. There, it is shown that the maximum of the distribution goes from left to right as the effective dimension is increased.

Our findings can be summarized by Fig. 3 and described as follows. In the small disorder regime, there is a crossover

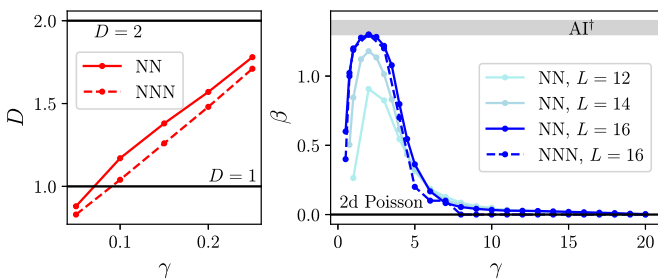


FIG. 3. Two transitions in the XXZ model with dissipative disorder. Hermiticity breaking (left): For $0.05 \leq \gamma < 0.25$, we find that the NN and NNN spectral statistics changes from those of 1d Poisson to 2d Poisson, and thus Hermiticity is broken first. Shown is the fitted effective dimensions D of the Poisson process for NN (full curve) and NNN (dashed curve). Data are shown for $L = 16$ spins in the $S_z = 0$ magnetization sector. Integrability breaking (right): For larger γ , i.e., $0.5 < \gamma < 20$, we find β yielding to a very good fit with the 2dCG. At $\gamma = 2$, the NN (full curve) and NNN (dashed curve) statistics are very close to those of AI^\dagger corresponding to $\beta \approx 1.3-1.4$ (horizontal band), representing a complete breaking of integrability. As γ is increased further, there is a crossover to the statistics of 2d Poisson (horizontal line at $\beta = 0$).

between the 1d Poisson statistics at $\gamma = 0$ —where our XXZ spin chain is integrable—towards the 2d Poisson statistics, which is well described by an increase in effective dimension, $1 \leq D < 2$. We reach up to $D \approx 1.7$ at $\gamma = 0.25$ for both NN and NNN spacing distributions. Therefore, Hermiticity is broken first on a smaller scale. This is summarized in Fig. 3 (left) and described in detail in Sec. III A.

For intermediate to large values of $\gamma = 0.5-20$, we see a rise from $\beta \approx 0.6$ at $\gamma = 0.5$ to $\beta \approx 1.3-1.4$ at $\gamma = 2$ where class AI^\dagger is located, to which we also compare. We see that integrability is broken as we approach the fully chaotic behavior characterized by random matrix class AI^\dagger . For larger γ , the disorder term (3) leads to an alignment of spins and thus again to a deterministic behavior, approaching 2d Poisson statistics with $\beta = 0$ around $\gamma \approx 8$; see Fig. 3 (right). This is discussed in Sec. III B, including the approach to class AI^\dagger with system size L in Sec. III B. The asymptotic approach to $\beta = 0$ in the range $\gamma = 8-20$ is discussed in Sec. III C, where we also use the surmise (7) for the finer scaling in the NN distribution. To complete the picture, we show and discuss results for the complex spacing ratios at various values of γ in Sec. III D.

A. Hermiticity breaking at small disorder γ : From 1d to 2d Poisson statistics

This section presents the regime of small γ , in the range $\gamma = 0-0.25$, and compares our model to Poisson statistics with varying dimension, given by Eqs. (9) and (10) for the NN and NNN spacing distribution, respectively; see Fig. 4. A representative of the corresponding spectrum is also shown—notice the different scales on the y axis—with the part of the spectrum that is used representing the bulk, highlighted in red. As explained in Sec. II, the spectrum is symmetric with respect to a line parallel to the real axis. This symmetry line changes with γ .

Starting with $\gamma = 0$ (left plots), the spectrum is real, the XXZ model is integrable, and we obtain a very good agreement with 1d Poisson statistics for both NN and NNN as expected. Notice that at $\gamma = 0$, the energies are doubly degenerate, which is why we only show spacings with $S_z = 0$ and parity $P = +1$ (for $L = 16$, this sector is of dimension 6470). The plots for $S_z = 0$ with $P = -1$ (for $L = 16$, this sector is of di-

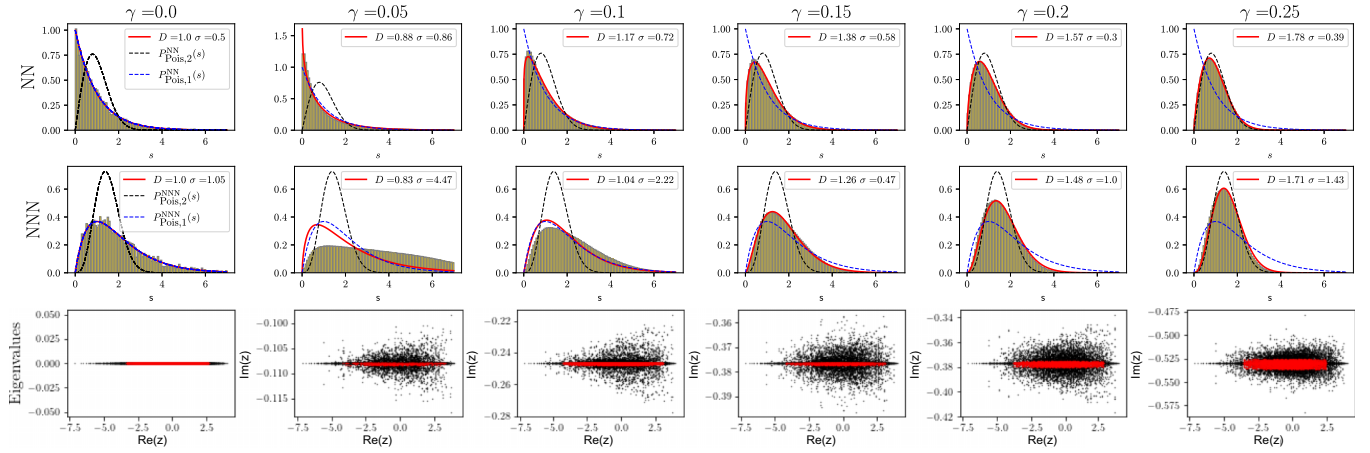


FIG. 4. The NN (top) and NNN spacing distribution (middle) of at least 490 disorder realizations, and scatter plot with selected eigenvalues highlighted in red for a single realization of the spectrum (bottom) for $\gamma = 0, 0.05, 0.1, 0.15, 0.2, 0.25$. In red (full line), we show (9) and (10) for the NN and NNN distribution, respectively, for the best-fit value for the effective dimension D , and indicate the corresponding standard deviation σ (in units of 10^{-2}). For comparison, we also show the results for $D = 1$ (blue dashed) and $D = 2$ (black dashed line). For pure XXZ, $\gamma = 0.0$, the spectrum is real and, since there is no disorder, the data shown are for a single realization. In addition, the full $S_z = 0$ is degenerate and splits into two sectors: an even-parity sector and an odd-parity one; we show statistics only for the even-parity sector. Switching on $\gamma > 0$, we see how these sectors start to mix, which may also be responsible for the disagreement of the NNN at the smallest values of $\gamma = 0.05$.

mension 6400) look similar. For our smallest value of $\gamma > 0$, we obtain a somewhat reasonable fit for the NN, with $D \approx 0.88$ consistent with $D = 1$. In contrast, the distribution for the NNN does not yield a good fit at all, a feature that persists for $\gamma = 0.1$. A possible explanation is that for these small values of γ , the spectrum is almost singular, being concentrated on a line parallel to the real line, with very few eigenvalues in the complex plane (see Fig. 5), and therefore the unfolding procedure described in Sec. V A for a 2d complex spectrum may not be completely suitable. For $\gamma = 0$, we used the 1d version of the unfolding method described in Sec. V A [55].

From $\gamma = 0.1$, both NN and NNN start to deviate from $D = 1$, and the best fits in D reach values up to $D \approx 1.7$ at $\gamma = 0.25$. Comparing NN and NNN leads to consistent values within a small margin. We thus believe that the fits to a one-parameter family of distributions are not a coincidence, but rather capture properties of an underlying effective Poisson interaction.

This leads to the interpretation that Hermiticity is broken first, while maintaining an (almost) integrable system, the characteristic of which is given by a Poisson distribution at intermediate dimension $1 < D < 2$. Increasing to the next higher value of $\gamma = 0.5$, detailed in the next Sec. III B, the maximum of the NN crosses to the right of the 2d Poisson distribution (at $\beta = 0$), which then fits the 2dCG. The fact that $D = 2$ is not fully reached by increasing γ here can be interpreted as a competition between Hermiticity and integrability breakings around the scale $\gamma = 0.25$ – 0.5 .

As an example for the crossover between one- and two-dimensional spectra, we show in Fig. 5 cuts through the spectral density perpendicular to the real axis at $x_0 \approx 0$ as a function of imaginary part y . Noting the difference in scale, we see that between $\gamma = 0.1$ and 0.2 shown here, the spectrum slowly softens and starts spreading into the complex plane. The difference in abundance of eigenvalues with a nonvanishing imaginary part may explain why the NNN distribution

in Fig. 4 fits well only from a certain value of $\gamma = 0.15$ onwards.

B. Integrability breaking at intermediate to large disorder γ : From 2d Poisson statistics to class AI^\dagger and back

In this section, we discuss the transition from random matrix statistics class AI^\dagger to 2d Poisson statistics, witnessed for intermediate ($\gamma = 0.5$) to large ($\gamma = 20$) disorder dissipation strength. The approach towards fully chaotic statistics represented by random matrix class AI^\dagger when increasing system size $L = 12, 14$, and 16 is included in Sec. III B below.

The smallest value of disorder for which a meaningful fit with a 2dCG at $\beta \geq 0$ can be made is $\gamma = 0.5$, when $\beta = 0.6$ (0.4) for NN (NNN); see Fig. 6 (left). At this disorder strength, both Hermiticity and integrability appear to be broken. The system is in between the integrable case ($\beta = 0$) and the fully chaotic case ($\beta \approx 1.3$ – 1.4 , equivalent to random matrix symmetry class AI^\dagger). The latter is then attained at $\gamma = 2$, where the maximal value for β (and height of the maximum) is reached; see Fig. 3 (right). We compare here the NN and NNN spacings with the 2dCG rather than AI^\dagger .

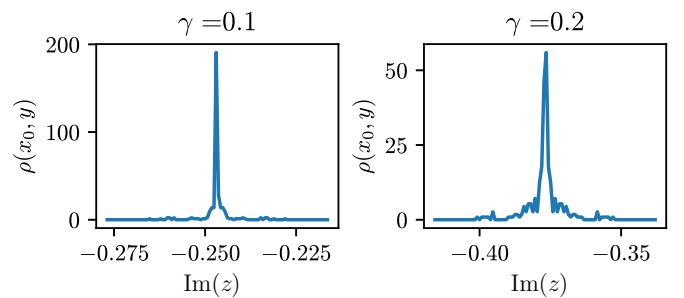


FIG. 5. Cuts through the spectral density (for a single realization) in imaginary direction at $x_0 \approx 0$, for $\gamma = 0.1$ (left) and $\gamma = 0.2$ (right).

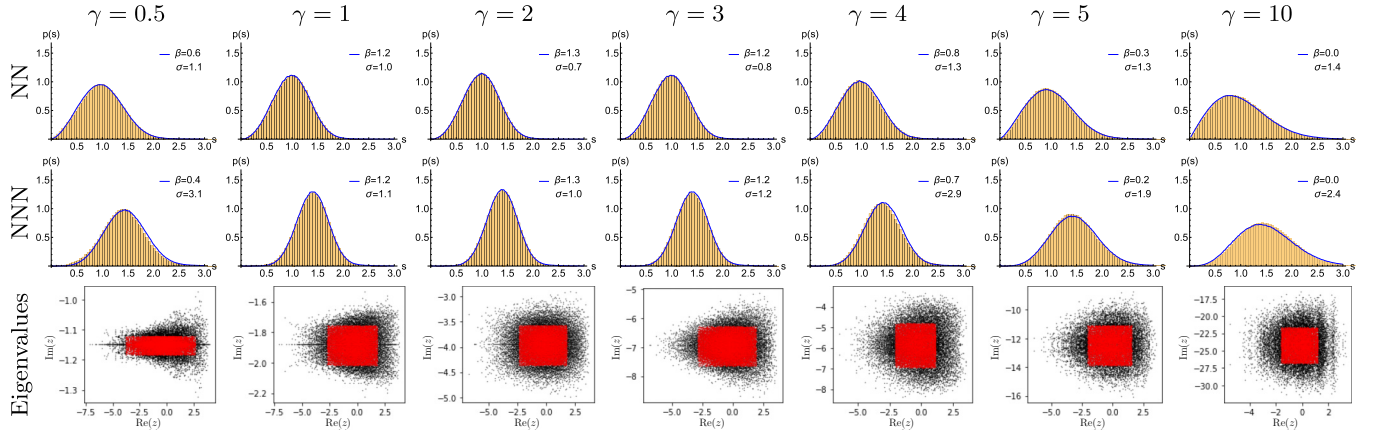


FIG. 6. Comparison of the model (1) with increasing dissipative order γ , with size $L = 16$ and spins in the $S_z = 0$ magnetization sector (histograms) for at least 450 realizations, and the best fit to the 2dCG (blue curves) of size $N = 5000$. The NN distribution is given in the first row, whereas the NNN spacing is shown in the second row. Additionally, we give the standard deviation σ in units 10^{-2} for each comparison of the spin-chain data with the 2dCG. In the bottom row, we show an example of the complex eigenvalue data for a single realization, with the points used in the statistics highlighted in red.

This is because the AI^\dagger class is very well approximated by the 2dCG at these values of β , as shown in Fig. 11 and Table IV. Furthermore, random matrix statistics is approached in β from below (see, also, the next Sec. III B) and the value of the standard deviation, σ (17), gives a measure of how close it is.

Increasing γ further leads to a rapid decrease in the best-fit value for β ; see, also, Table I below. From $\gamma \simeq 8$ –10 onwards, we consistently obtain $\beta = 0$. This is because the disorder is so strong that the spins become aligned and the statistics again becomes deterministic. The best fits for β for NN and NNN and corresponding values, including standard deviations, are collected in Table I. In this section, we only fit to β in the 2dCG where the step width is 0.1, but both NN and NNN distributions are available. The next Sec. III C presents a much finer fit in β for $\gamma \geq 8$, which is only possible for the NN thanks to the surmise (7), which is a very good approximation close to $\beta = 0$. The approach to zero can also be clearly seen in the summary in Fig. 3 (right). Similar findings for Hermitian Hamiltonians comparing to 1d Poisson and corresponding classical random matrices, using both NN and NNN spacings, were very recently made [56].

The findings in this section correspond to the expected behavior of a quantum chaotic system with imaginary disorder, where the spectral statistics lies between 2d Poisson and the corresponding random matrix symmetry class, in accordance with the GHS conjecture.

TABLE I. List of best-fit β for the comparison of the NN spacing and NNN spacing of the spin chain with $L = 16$ and $\gamma = 0.5, 0.75, 1, 2, \dots, 20$ to the 2dCG and the corresponding standard deviation σ in units of 10^{-2} . Notice that apart from $\gamma = 0.5$, the values obtained for β from NN and NNN agree or differ by only 0.1.

	γ	0.5	0.75	1.0	2.0	3.0	4.0	5.0	6.0	7.0	8.0	9.0	10.0	11.0	12.0	13.0	14.0	15.0	16.0	17.0	18.0	19.0	20.0
NN	β	0.6	1.0	1.2	1.3	1.2	0.8	0.3	0.2	0.1	0.1	0.0	0.0	0.0	0.0	0.0	0.0	0.0	0.0	0.0	0.0	0.0	0.0
	σ	1.1	1.3	1.0	0.7	0.8	1.3	1.3	1.3	1.3	1.7	1.6	1.4	1.4	1.3	1.3	1.2	1.2	1.0	0.9	0.9	0.8	0.8
NNN	β	0.4	1.0	1.1, 1.2	1.3	1.2	0.7	0.2	0.1	0.1	0.0	0.0	0.0	0.0	0.0	0.0	0.0	0.0	0.0	0.0	0.0	0.0	0.0
	σ	3.1	1.5	1.1	1.0	1.2	2.9	1.9	1.6	2.6	2.8	2.6	2.4	2.4	2.3	2.2	2.1	2.0	1.9	1.7	1.6	1.4	1.3

Dependence on system size L

The main data presented so far are always for the longest spin chain, with $L = 16$. This corresponds to a Hilbert space dimension of 12 870, which allows reaching a fully chaotic behavior. Here, we also present data for system sizes $L = 14$ and $L = 12$, with respective dimensions of Hilbert space 3432 and 924, at the values $\gamma = 2$ and $\gamma = 20$. The limit towards random matrix statistics of class AI^\dagger is not reached for all system sizes (Fig. 7), but the 2d Poisson limit is reached fully at large $\gamma = 20$ for all three system sizes (see Fig. 8).

At the very beginning of this section, we have reminded the reader that in the β range between 2d Poisson statistics and class AI^\dagger , the latter has the highest maximum for the NN spacing at the highest value of $\beta \approx 1.3$ –1.4. In all three systems sizes, we observed that the highest maximum is obtained for disorder strength $\gamma = 2$, thus being the closest to class AI^\dagger . This is why, to look at the dependence on the system size L , we can focus on a single disorder strength. Figure 7 shows that the best fit for β at $\gamma = 2$ increases with system size, and only reaches $\beta = 1.3$ for the largest systems. This is summarized in Table II. Notice that the maximal disorder found at $\gamma = 2$ is not apparently related to any symmetry of the Hamiltonian.

C. Asymptotic approach to 2d Poisson statistics for large disorder γ

This section details the asymptotic approach to 2d Poisson statistics $\beta \rightarrow 0$ for large values of $\gamma = 8$ –20. Because for the

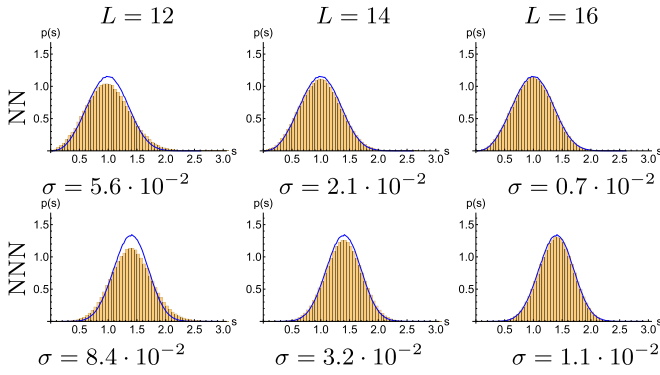


FIG. 7. Comparison of the XXZ with dissipative disorder $\gamma = 2$ in the $S_z = 0$ magnetization sector with increasing number of spins, $L = 12, 14, 16$ (from left to right, histograms) and the symmetry class AI^\dagger of complex symmetric matrices (blue curve) of size $N = 5000$. The NN distribution is given in the first row, whereas the NNN spacing is shown in the second row. Additionally, we give the standard deviation σ between the two plotted distributions below each plot. We observe a decrease of the standard deviation for growing L , as expected.

2dCG we have only discrete steps in β of size 0.1 available, we will use the surmise (7) instead here. It is an excellent approximation for the local statistics close to $\beta = 0$, but it only allows fitting the NN spacing distributions. Figure 9 shows fits in β of the surmise to the NN spacing distribution for various values of $\gamma = 8\text{--}20$ in steps of size 2 (or more). The fitted β values for all values of $\gamma \geq 8$, together with the corresponding standard deviations, are provided in Table III.

D. Comparison to complex spacing ratio discussion

Section V B introduces the complex spacing ratios u . Their probability density, as seen in Fig. 10, contains interesting patterns, especially in the chaotic regime: the lower density around the origin and around $r = 1$ is due to level repulsion. It is not likely for an eigenvalue and its NN to be close together, thus the density is lower at $r = 0$; and an eigenvalue's NN and NNN would most likely lie on either side of it, making the density lower at $r = 1$; see, also, Fig. 12, which compares the complex spacing ratio distribution of 2d Poisson statistics with that of class AI^\dagger . The “bow and arrow” feature seen for small

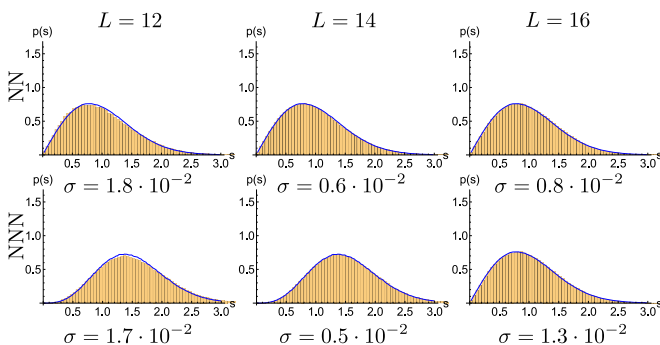


FIG. 8. Same comparison as in Fig. 7, but at $\gamma = 20$ (histograms), where all three system sizes agree with 2d Poisson statistics (blue curves). Here, σ is comparable for all three system sizes.

TABLE II. Best fits for β at the same disorder strength $\gamma = 2$ for different system sizes L , with standard deviation σ in units 10^{-2} .

Size	L	12	14	16
NN	β	0.9	1.2	1.3
	σ	1.3	0.6	0.7
NNN	β	0.8	1.1	1.3
	σ	3.5	1.3	1.0

γ is a manifestation of an underlying structure of the complex eigenvalues. As observed and explained in Appendix D of [57], this feature is a result of an eigenvalue's NN and NNN being on the real line and as complex conjugate to it, or vice versa. Section II B showed that the Hamiltonian is pseudo-Hermitian and thus its spectrum is symmetric to reflection across a line parallel to the real axis. In the complex spacing ratios, this symmetry manifests itself as reflection symmetry across the real axis. Additionally, the excess of ratios along the real line is a result of real eigenvalues having real NN and NNN.

IV. SPECTRAL STATISTICS OF COMPLEX EIGENVALUES

In this section and in the next, we describe the tools that we used to analyze our results in the previous section. In particular, we introduce and compare two different random point processes of N points z_1, \dots, z_N in the complex plane (including the real line as a special case), namely, the 2dCG and the D -dimensional Poisson point process, in addition to the class AI^\dagger , which can be well approximated by the 2dCG with $\beta = 1.4$ [46]. These processes are characterized by a joint distribution $\mathcal{P}_N(z_1, \dots, z_N)$. We will recall exact and approximate analytical expressions, as well as numerically generated distributions for the local spacing between complex eigenvalues.

The NN is given for each point z_i by finding the NN in radial (Euclidean) distance as $s_i^{\text{NN}} = \min_{j \neq i} |z_i - z_j|$, being realized, say, by $j = i_0$ [58]. The NNN is then at distance $s_i^{\text{NNN}} = \min_{j \neq i, i_0} |z_i - z_j|$. When determining the respective distributions numerically, we first normalize the mean density by unfolding, as described in Sec. V A, and then determine the NN and NNN for all $i = 1, \dots, N$ to obtain a distribution. We will be careful to only take points inside the so-called bulk of the spectrum, which are sufficiently away from the edge of the spectrum—of the order of $O(1/\sqrt{N})$ for the random matrix ensembles that we study. In all our examples, the spectral density has compact support [59].

A. The two-dimensional Coulomb gas and a surmise

The first example of a point process that we compare our data with is the 2dCG, featuring a logarithmic interaction among the N point charges, with a strength that can be interpreted as an inverse temperature β . Choosing a Gaussian confining potential, the joint distribution in the complex plane reads

$$\mathcal{P}_{N,\beta}(z_1, z_2, \dots, z_N) \propto \exp \left[- \sum_{i=1}^N |z_i|^2 + \frac{\beta}{2} \sum_{i \neq j}^N \ln |z_i - z_j| \right]. \quad (6)$$

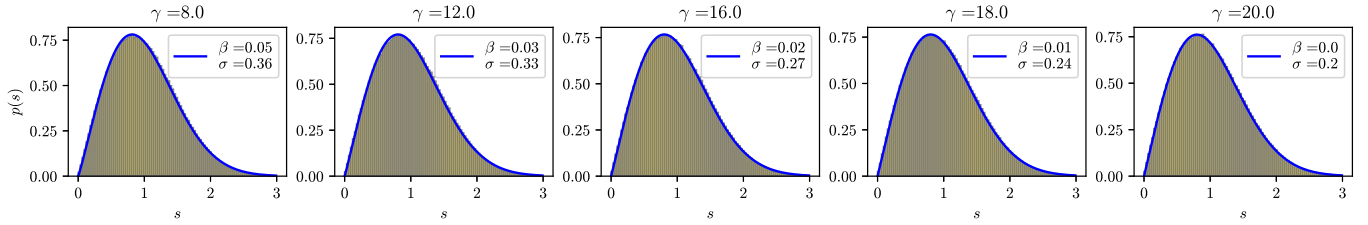


FIG. 9. Asymptotic approach to 2d Poisson statistics for large disorder strength γ . The histograms for the NN spacings of at least 450 realizations of the spin chain with $L = 16$ in the $S_z = 0$ magnetization sector are compared with the best-fit β of the surmise (7) shown as a smooth blue line. The legend shows the value of β and the standard deviation (in units of 10^{-2}) of the fit.

The normalization constant is given by the complex Selberg integral, which can be solved analytically only for $\beta = 0$ or 2. Compared to the standard statistical mechanics notation, where the Gaussian term has a coefficient $\beta/2$, the positions of the point charges are rescaled as $z_i \rightarrow \sqrt{2/\beta} z_i$. This rescaling allows us to take the limit $\beta \rightarrow 0$ and thus to recover the 2d Poisson case [60]. In addition, the three different local symmetry classes of non-Hermitian random matrices can be obtained: namely, Eq. (6) with $\beta = 2$ corresponds to the complex eigenvalue distribution of the complex Ginibre ensemble (class A), which can be solved analytically; cf. the Appendix. In turn, $\beta = 1.4$ and $\beta = 2.6$ give a very good approximation of the NN spacing distribution of class AI^\dagger and class AII^\dagger , respectively [46]. Below, we will show that this approximation also extends to NNN. To date, no analytic results for the local NN and NNN spacing are known apart for $\beta = 0, 2$ [61]. The numerically determined spacings in the 2dCG are shown in Fig. 2(b).

Interestingly, in the vicinity of $\beta = 0$, the NN spacing distribution of the 2dCG can be well approximated by a surmise [46] based on 2×2 matrices. As a function of β , it is given by [62]

$$p_{\text{NN},\beta}^{\text{surmise}}(s) = \frac{2\alpha_{\text{eff}}^{1+\beta_{\text{eff}}/2}}{\Gamma(1+\beta_{\text{eff}}/2)} s^{1+\beta_{\text{eff}}} \exp[-\alpha_{\text{eff}} s^2],$$

$$\alpha_{\text{eff}} = \frac{\Gamma^2[(3+\beta_{\text{eff}})/2]}{\Gamma^2(1+\beta_{\text{eff}}/2)}, \quad (7)$$

where

$$\beta_{\text{eff}}(\beta) = 2.108\beta - 0.19\beta^2 + 0.03\beta^3. \quad (8)$$

This effective β is introduced to improve the approximation to the true 2dCG up to approximately $\beta = 0.5$; see the discussion in [46]. Setting $\beta = 0$ in (7) exactly reproduces the NN spacing distribution (9) for 2d Poisson statistics. The distribution $p_{\text{NN},\beta}^{\text{surmise}}(s)$ and its first moment are again normalized to unity. Even at larger values of β , this surmise, while approximate, can be very useful to do a first fit of β that can

then be improved by finding the best fit to the (numerically generated) spacings of the true 2dCG.

We note in passing that when restricting all points in (6) to the real line, the joint density of real eigenvalues is that of the common Hermitian Gaussian random matrix ensembles, i.e., GOE, Gaussian unitary and symplectic ensemble, at respective values $\beta = 1, 2, 4$ (see, e.g., [63]). This is also known as a Dyson gas. In addition to these values, where the ensemble can be solved analytically and the statistics is well understood, the general case $\beta > 0$ has been well studied [64] (and the normalizing Selberg integral is then known for any N and β). In this Hermitian setup, a popular tool is the Wigner surmise based on 2×2 matrices, well approximating the local NN spacing distribution for $\beta = 1-4$ away from 1d Poisson statistics at $\beta = 0$. All three Hermitian ensembles have distinct local statistics and exhaust the three random matrix bulk statistic classes for real eigenvalues. This is in stark contrast to the three non-Hermitian Ginibre ensembles with real, complex, and quaternion elements, since these three share the same local statistics in the bulk of the spectrum away from the real line, as shown analytically in [21,65].

B. The D -dimensional Poisson point process

The second point process we compare our data to is the Poisson point process in D dimensions, which has been much studied in the literature. It is given by N points distributed randomly and independently in a D -dimensional ball of radius R , keeping the density of points fixed by setting $N/R^D = 1$. The joint distribution $\mathcal{P}_N(z_1, \dots, z_N)$ for Gaussian random variables thus corresponds to (6) at $\beta = 0$, and completely factorizes. After appropriate rescaling, the NN spacing distributions in $D = 2$ [6] and for general D [47] can be derived analytically in the large- N limit, yielding

$$P_{\text{Pois},D}^{\text{NN}}(s) = D \Gamma\left(1 + \frac{1}{D}\right)^D s^{D-1} e^{-\Gamma(1+\frac{1}{D})^D s^D}. \quad (9)$$

At $D = 1$, it recovers the familiar exponential distribution $P_{\text{Pois},1}^{\text{NN}}(s) = e^{-s}$, whereas at $D = 2$, it is Gaussian with a linear prefactor stemming from the area measure; see, also, [66]. In

TABLE III. List of best-fit β for the comparison of the NN spacing of the spin chain with $L = 16$ and $\gamma = 8, \dots, 20$ to the NN 2dCG surmise (7) and the corresponding standard deviation σ in units of 10^{-2} .

γ	8	9	10	11	12	13	14	15	16	17	18	19	20
NN β	0.0547	0.0413	0.0337	0.0283	0.0273	0.026	0.023	0.0196	0.0169	0.0135	0.0108	0.0066	0.0035
σ	0.36	0.35	0.33	0.35	0.33	0.33	0.31	0.3	0.27	0.24	0.24	0.21	0.2

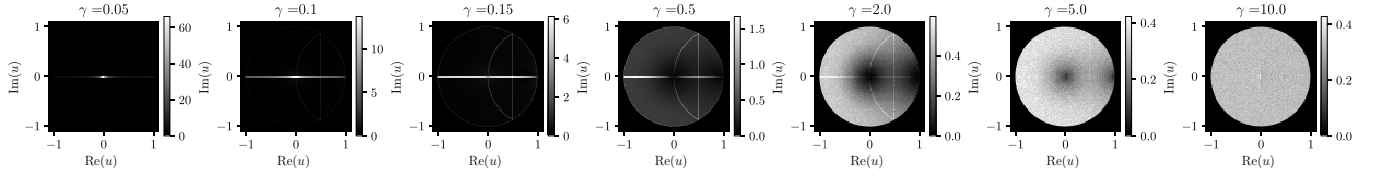


FIG. 10. Histograms of complex spacing ratio (16) for the XXZ model with dissipative disorder (1) with $L = 16$ spins in the $S_z = 0$ sector, for various values of disorder strength γ . For each value of γ , the data shown are for at least 450 realizations, in the bulk of the spectrum.

turn, the NNN spacing distribution can be derived by integrating over the joint distribution of NN and NNN, provided in, e.g., [47], to find

$$P_{\text{Pois},D}^{\text{NNN}}(s) = D \Gamma\left(1 + \frac{1}{D}\right)^{2D} s^{2D-1} e^{-\Gamma(1+\frac{1}{D})^D s^D}. \quad (10)$$

Both distributions are normalized to unity. The NN distribution is rescaled to have its first moment equal to one, and the NNN distribution is rescaled by the very same factor. Based on the BT conjecture, generic integrable Hamiltonian systems are expected to display Poisson statistics at $D = 1$ when being Hermitian, and $D = 2$ Poisson statistics when non-Hermitian; see, e.g., [21,47]. Because of this, we assume that both 2d Poisson NN and NNN spacings describe the spectral data of such Hamiltonians. This was numerically confirmed very recently for the BT conjecture in 1d in [56].

Since both distributions (9) and (10) are analytic in D , we can continue them to arbitrary $D > 0$, as illustrated in Fig. 2(a). Such a Poisson distribution with an effective dimension $1 < D < 2$ was observed, e.g., on forest patches; cf. [25].

C. Non-Hermitian random matrix class AI^\dagger

According to the GHS conjecture, fully chaotic non-Hermitian Hamiltonians follow local non-Hermitian random matrix statistics; therefore, we have to compare our model (1) to the random matrix ensemble corresponding to the same symmetry class. In Ref. [14], it was conjectured, based on numerical simulations, that among all 38 classes of non-Hermitian random matrices, there are only three different classes of local level spacing statistics in the bulk of the spectrum. Following their notation, representatives of these three different symmetry classes are given by the complex Ginibre ensemble (class A), Gaussian complex symmetric (class AI^\dagger), and complex self-dual (class AII^\dagger) matrices. The joint density is known only for class A, corresponding to (6) with $\beta = 2$.

Since our Hamiltonian (1) is also complex symmetric, as shown in Sec. II, we compare the NN and NNN spacing distributions with those of random matrices in class AI^\dagger . Such matrices are defined by symmetric $N \times N$ matrices J with complex elements and Gaussian distribution,

$$J = J^T, \quad P_N^{(\text{AI}^\dagger)}(J) = C_N e^{-\text{Tr}(JJ^\dagger)}, \quad (11)$$

with normalization $C_N^{-1} = \pi^N (\pi/2)^{N(N-1)/2}$. Apart from $N = 2$ [14,23] and the local limiting spectral density of rescaled imaginary parts (weak non-Hermiticity) [67], there are no analytic results available for local statistics in this class so far. While $N = 2$ is a good approximation for the Wigner surmise for Hermitian random matrices, it does not work here [46]. So

we have to generate the spacing distributions numerically; see Fig. 11.

It was found in [46] that the NN spacing distribution of class AI^\dagger can be very well fitted by a 2dCG at $\beta = 1.4$, which is also numerically generated; see the next Sec. IV A. In this work, we also compare to the NNN spacing of AI^\dagger , at the same value of $\beta = 1.4$, and find an excellent agreement; see Fig. 11 (right). The quality of the best fit for β (bold numbers) is shown in standard deviations σ (17) and Kolmogorov-Smirnov distances d (18) in Table IV, to be introduced in Sec. V C. The results for class A are presented in Table V.

These results further corroborate that the AI^\dagger random matrix symmetry class is very well approximated by a 2dCG. The same conclusion applies to the NNN spacing distribution of class AII^\dagger , shown in the Appendix, where we also discuss the quality of the fit comparing numerically generated spacings from class A with its analytic results.

V. METHODS

This section presents the methods we use to study and analyze the spectral statistics of the physical model, including unfolding, complex spacing ratio statistics, and fitting procedures.

A. Unfolding complex spectra

When comparing data from physics (or other sciences), e.g., taken by discrete (energy) eigenvalues E of Hermitian or non-Hermitian Hamiltonians, to universal predictions, e.g., from Poisson or random matrix statistics, some preprocessing is needed. Typically, the mean spectral density $\bar{\rho}(E)$ of the physical system contains model-specific (and physical) information. In order to have a chance to see universal statistics, one has to separate scales in the density $\rho(E)$ between the

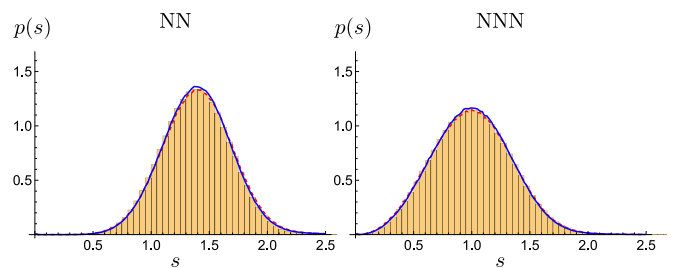


FIG. 11. The NN (left) and NNN (right) AI^\dagger spacing distribution generated numerically (histograms) for 500 random matrices of size $N = 5000$. Also shown are comparisons to the NN and NNN spacing distribution of the 2dCG, with fitted values $\beta = 1.3$ (red dashed) and $\beta = 1.4$ (blue full curve). The comparison with NNN is new here.

TABLE IV. List of standard deviations σ and Kolmogorov-Smirnov distances d (both in units 10^{-2}) between NN and NNN spacings of AI^\dagger and 2dCG, with $\beta \in [1.1, 1.6]$ in steps of 0.1. For NN, both measures favor $\beta = 1.4$ as the best fit, as does the Kolmogorov-Smirnov distance for NNN, whereas the standard deviation for the latter is best for $\beta = 1.3$ (bold numbers).

Fitted	β	1.1	1.2	1.3	1.4	1.5	1.6
NN	σ	3.3	2.2	1.1	0.9	1.7	2.7
	d	1.7	1.2	0.6	0.3	0.7	1.2
NNN	σ	3.4	2.0	0.8	1.4	2.7	4.0
	d	3.0	1.8	0.8	0.6	1.7	2.7

mean density and the fluctuation (fl) around the mean (also called local or microscopic),

$$\rho(E) = \bar{\rho}(E) + \rho_{\text{fl}}(E). \quad (12)$$

For geometric reasons, with N the number of points and $\bar{\rho}(E) \sim N$, these fluctuations are typically of the order of $1/N$ in 1d and of order of $1/\sqrt{N}$ in 2d, at least in the bulk of the spectrum.

The removal of the mean density or, in other words, map to a normalized constant density, is called unfolding. In 1d, this is a unique and well-understood procedure; see, e.g., [68]. In 2d, however, there is more freedom and several different methods have been proposed, e.g., [14,18,21,41,57,69]. We follow the procedure described in [21], which we briefly recall below.

We start from the exact density of states of N eigenvalues $z_{i=1,\dots,N}$ in 2d or the complex plane given by

$$\rho(x, y) = \frac{1}{N} \sum_{i=1}^N \delta^{(2)}(z - z_i), \quad (13)$$

where $z = x + iy$. The mean, or average, density of states can be approximated by a smooth function by replacing each $\delta^{(2)}$ function with a Gaussian distribution with a certain variance Σ ,

$$\bar{\rho}(x, y) = \frac{1}{2\pi \Sigma^2 N} \sum_{i=1}^N e^{-\frac{|z-z_i|^2}{2\Sigma^2}}. \quad (14)$$

Here, $\Sigma = \alpha \bar{s}$ is determined by multiplying the average NN spacing of the spectrum, \bar{s} , by a constant α of $O(1)$ in order to smear over several eigenvalues on average [70]. The unfolded NN and NNN spacings s_i^{NN} and s_i^{NNN} are then defined by

TABLE V. Standard deviations σ and Kolmogorov-Smirnov distances d (both in units 10^{-2}) between numerically generated NN and NNN spacings of class A and the numerically generated 2dCG at $\beta = 2$.

$\beta = 2$	NN	NNN
σ	0.44	1.4
d	0.2	1.2

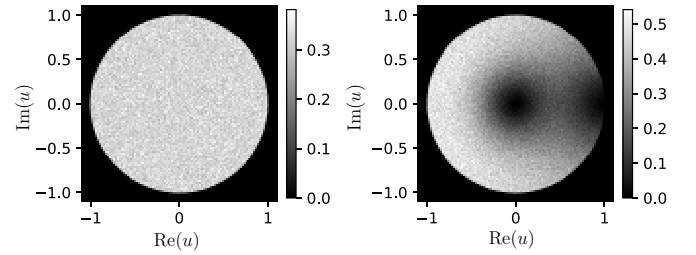


FIG. 12. Numerically generated complex spacing ratio distribution $R(u = re^{i\theta})$ for 2d Poisson (left) and random matrices in class AI^\dagger (right). Both plots are based on size $N = 5000$, with 500 realizations. Class AI^\dagger looks qualitatively similar to class A, with a pronounced hole at the origin and depletion from unity; see [19,47].

removing the local scale, that is, by multiplying the original spacings by the same factor,

$$s_i^{\text{NN}} = |z_i - z_i^{\text{NN}}| \sqrt{\bar{\rho}(x_i, y_i)}, \quad (15a)$$

$$s_i^{\text{NNN}} = |z_i - z_i^{\text{NNN}}| \sqrt{\bar{\rho}(x_i, y_i)}, \quad (15b)$$

where z_i^{NN} is the NN to eigenvalue z_i , and z_i^{NNN} the NNN. After unfolding, we normalize the NN spacing such that the first moment is equal to one and measure the NNN spacing on the same scale.

B. Complex spacing ratios

Alternatively to the NN (and NNN) spacing distribution, a tool that does not require unfolding relies on the spacing ratios, as proposed in 1d [27] and 2d [47]. In 2d, the complex spacing ratio is defined as

$$u_i = \frac{z_i^{\text{NN}} - z_i}{z_i^{\text{NNN}} - z_i}, \quad (16)$$

and the goal is to provide (analytical) predictions for the limiting probability distribution $R(u = re^{i\theta})$ as a function of radius r and angle θ . For example, the 2d Poisson process has a flat distribution over the unit disk, $R_{\text{Pois}}(u) = \Theta(1 - |u|)/\pi$, as shown in Fig. 12 (left). In view of the difficulties to make 2d fits to such ratios, the radial and angular distributions were also introduced, respectively, by averaging $R(u = re^{i\theta})$ over angle θ or radius r . Moments were computed for the complex Ginibre ensemble class A [47] and for classes AI^\dagger and AII^\dagger [19].

In 1d, the joint density and its normalization are well understood. This has led to a plethora of predictions for limiting ratios (cf. [71]), including for further neighbors and, most importantly, for their dependence on the inverse temperature β in the Dyson gas.

In contrast, in 2d, the only approximate results for radial and angular moments are known for class A [72], which is not the symmetry class of our model. For the random matrix class AI^\dagger applicable here, complex spacing ratios (16) can be computed numerically (see Fig. 12, right), as well as the corresponding radial and angular moments [19]. However, it is not clear what the transition between the 2d Poisson statistics and class AI^\dagger would look like. Moreover, in the analysis of data from ecology [25], the behavior of radial and angular moments with effective β between the 2d Poisson statistics

and class. A random matrix predictions was found to be inconclusive. For this reason, we did not pursue a quantitative comparison between our data and complex spacing ratios.

C. Comparison of numerical data

In order to compare the spectral distributions of the spin-chain model with dissipative disorder to those from the Poisson, 2dCG, or random matrix of class AI^\dagger , we present two measures of agreement between two distributions $p_1(s)$, $p_2(s)$. Both measures are based on numerical data. The first one is the *standard deviation* σ , defined as

$$\sigma = \left\{ \frac{1}{n} \sum_{j=1}^n [p_1(s_j) - p_2(s_j)]^2 \right\}^{\frac{1}{2}}, \quad (17)$$

where n is the number of bins in the data, and $p_1(s_j)$ and $p_2(s_j)$ are the number of counts in the j th bin at its midpoint s_j in each distribution. Hence, one first determines a fine binning of the data into a histogram, and then uses these histogram points $(s_j)_{j=1}^n$ for the comparison. The sum was cut off at $s = 3$ when fitting to the 2dCG because of the exponential suppression, and at a larger $s = 7$ when fitting to a generalized D -dimensional Poisson process.

The second measure is the so-called *Kolmogorov-Smirnov distance* d , which is defined as

$$d = \max_{x \geq 0} |F_1(x) - F_2(x)| \in [0, 1], \quad (18)$$

between the cumulative distributions F_1 and F_2 of distributions p_1 and p_2 , respectively. It is independent of the binning into histograms. However, the calculations take much longer than the ones for the standard deviation. We checked that the Kolmogorov-Smirnov distances and the standard deviations have the same sensitivity to, e.g., β for the comparison of the spin-chain data and the 2dCG.

As a reference, we generated complex eigenvalues from class A (of size $N = 5000$), even though it exactly corresponds to the 2dCG with $\beta = 2$. The density of class A and the 2dCG is flat for large N , and thus no unfolding is needed [6,18,21]. Such fits, presented in Table V, serve as a comparison to judge the quality of the other best fits for matrices of this size in the other two classes, AI^\dagger and AII^\dagger [73].

The values obtained for σ and d for class AI^\dagger (Table IV) and for class AII^\dagger (Table VI) are comparable to that of class A (which we know exactly). For the comparison, we used the library of spacings in the 2dCG that was generated numerically in [21] with $N = 200$ point charges. It was subsequently increased to $N = 5000$ in [46] to improve the statistics of our Coulomb data, in particular in the vicinity of $\beta = 0$. Note that the best fit for the NNN is systematically less good than for the NN data. This could come from the maxima of the NNN curves, which are always larger than the NN curves. The maxima of the distribution being larger, they could sum into larger deviations and thus yield a larger maximal difference for the cumulative distribution function.

VI. CONCLUSIONS

Using the NN and NNN distributions, this work shows that the XXZ model with dissipative disorder exhibits two spectral

crossovers as a function of disorder strength γ . At $\gamma = 0$, the model is a pure integrable XXZ spin chain and its spectral statistics (once restricted to an appropriate symmetry sector to avoid exact degeneracies) corresponds to the 1d Poisson statistics. As the dissipative disorder strength is increased, but still small, the spectrum begins spreading into the complex plane and the statistics, approximately still integrable, are close to Poisson with an effective dimension $D > 1$. As the dissipative disorder is increased further, integrability begins to break and both the NN and NNN distributions are well fitted by the 2dCG with $\beta > 0$. At $\gamma = 2$, the model becomes fully chaotic with NN and NNN spectral statistics close to those of random matrices of class AI^\dagger , which is in the same non-Hermitian symmetry class as our model. Beyond $\gamma > 2$, we observe a crossover from chaos to integrability. The same crossover from chaos to integrability was detected in [44] through real singular-value statistics and is now also validated from complex spectral analysis. In a similar manner to the Hermitian case, increasing the dissipative disorder induces a crossover of the spectral statistics from chaotic—described by random matrix symmetry class AI^\dagger or the 2dCG statistics with $\beta \approx 1.3$ – 1.4 —to integrable—described by the statistics of the 2d Poisson point process (or, equivalently, by the 2dCG with $\beta = 0$). We tracked the crossover by fitting the NN and NNN spectral distributions to the corresponding value of β in the 2dCG, obtaining a consistent value for β from both fits. We complement this analysis by also studying the complex spectral ratios as a function of the disorder.

ACKNOWLEDGMENTS

We acknowledge funding from the John Templeton Foundation (JTF Grant No. 62171) and the Luxembourg National Research Fund (FNR, Attract Grant No. 15382998). F.R. acknowledges financial support from the Fulbright Research Scholar Program. The opinions expressed in this publication are those of the authors and do not necessarily reflect the views of the JTF. The numerical simulations presented in this work were in part carried out using the HPC facilities of the University of Luxembourg. This work was partly supported by the Deutsche Forschungsgemeinschaft (DFG) Grant No. SFB 1283/2 2021–317210226 (G.A., P.P.) and a Leverhulme Trust Visiting Professorship, Grant No. VP1-2023-007 (G.A.). G.A. is indebted to the School of Mathematics, University of Bristol, where this research was conducted. A.C. acknowledges the CNLS at Los Alamos National Laboratory, where part of this research was conducted.

APPENDIX: RANDOM MATRIX BULK SYMMETRY CLASSES

This Appendix briefly recalls what is known about local statistics in non-Hermitian random matrix theory. We focus on the three symmetry classes that are conjectured to exhaust the local bulk statistics [14]. Representatives for these three bulk symmetry classes are classes A, AI^\dagger , and AII^\dagger . We present NN and NNN spacing distributions and compare to the 2dCG, with the class AI^\dagger being analyzed in Sec. IV C. Our new results include a comparison of the respective NNN with a fit to the 2dCG with the *same* β , for class AI^\dagger in Fig. 11

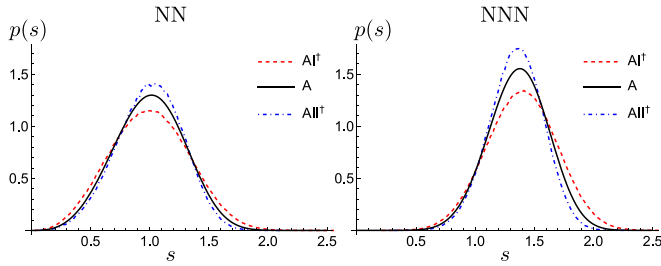


FIG. 13. The NN (left) and NNN (right) spacing distributions of the three random matrix symmetry classes. Namely, in order of increasing maxima, class AI^\dagger (red dashed line), class A (black full line), and class AII^\dagger (blue dash-dotted line). These, respectively, correspond to an increasing $\beta \approx 1.3$ – 1.4 , $\beta = 2$, and $\beta \approx 2.5$ – 2.6 .

(right) and for AII^\dagger in Fig. 14 (right). For illustration, we also compare the NN and NNN distributions of all three random matrix classes in Fig. 13 above. Note that based on perturbation theory, it was shown in [6,74] that for small spacings, the repulsion is cubic, $p(s) \sim s^3$, irrespective of the presence or absence of time-reversal symmetry.

1. Class A - Definition and analytic results

The simplest and best understood is class A, the complex Ginibre ensemble, consisting of complex non-Hermitian $N \times N$ random matrices $J \neq J^\dagger$ with independent Gaussian elements and no further symmetry,

$$P_N^{(A)}(J) = C_N e^{-\text{Tr}(JJ^\dagger)}, \quad C_N^{-1} = \pi^{N^2}. \quad (\text{A1})$$

Its joint distribution of complex eigenvalues exactly corresponds to the 2dCG (6) at $\beta = 2$. So it represents a determinantal point process, and all complex eigenvalue correlation functions are known explicitly at finite and large N . The NN [11] and NNN [75] spacing distributions in the large- N limit read

$$p_{\text{NN}}^{(A)}(s) = E_{\text{NN}}^{(A)}(s) \sum_{j=1}^{\infty} \frac{2s^{2j+1} e^{-s^2}}{\Gamma(1+j, s^2)}, \quad (\text{A2})$$

$$p_{\text{NNN}}^{(A)}(s) = E_{\text{NNN}}^{(A)}(s) \sum_{j,k=1; k \neq j}^{\infty} \frac{\gamma(1+j, s^2)}{\Gamma(1+j, s^2)} \frac{2s^{2k+1} e^{-s^2}}{\Gamma(1+k, s^2)}, \quad (\text{A3})$$

where

$$\gamma(1+k, s^2) = \int_0^{s^2} t^k e^{-t} dt, \quad (\text{A4})$$

$$\Gamma(1+k, s^2) = \Gamma(1+k) - \gamma(1+k, s^2) \quad (\text{A5})$$

are the lower and upper incomplete Gamma function. Furthermore,

$$E_{\text{NN}}^{(A)}(s) = \prod_{j=1}^{\infty} \frac{\Gamma(1+j, s^2)}{\Gamma(j+1)} \quad (\text{A6})$$

is the so-called gap probability in class A to find an eigenvalue at the origin and the closest nonzero complex eigenvalue at radial distance s . For finite N , the sums and product in (A2)–(A6) extend only to $N-1$. The product converges very rapidly and can be truncated at, say, $N=20$. It is also clear

TABLE VI. List of standard deviations σ and Kolmogorov-Smirnov distances d (both in units 10^{-2}) between NN and NNN spacings of AII^\dagger and 2dCG, with $\beta \in [2.3, 2.8]$ in steps of 0.1. For NN, the best fit is with $\beta = 2.6$ for both distances, as it is for the NNN for σ , whereas d favors $\beta = 2.5$ for NNN (bold numbers).

Fitted	β	2.3	2.4	2.5	2.6	2.7	2.8
NN	σ	3.4	2.8	2.4	2.3	2.4	3.0
	d	1.4	1.1	1.0	0.9	1.0	1.2
NNN	σ	5.5	4.6	4.1	3.9	4.3	4.9
	d	2.8	2.1	1.6	1.9	2.4	2.8

from this formula that $N=2$ is not a good approximation here, as was already noted in [11]. Both spacing distributions (A2) and (A3) are normalized to unity. However, the first moment still has to be rescaled to unity, by numerically computing $s_1 = \int_0^\infty s p_{\text{NN}}^{(A)}(s) ds$, and then rescaling $p_{\text{NN}}^{(A)}(s) \rightarrow s_1 p_{\text{NN}}^{(A)}(s_1 s)$. After doing the same rescaling of (A3) with the same factor s_1 , the resulting distributions are shown in Fig. 13, left and right, middle curves; see, also, Fig. 2(b), left and right, with class A being given by the curve with the intermediate maximum.

2. Class AII^\dagger - Definition and fits to NN and NNN

We turn to the definition of the symmetry class AII^\dagger . The ensemble consists of non-Hermitian matrices of complex self-dual matrices J with quaternion elements, that we represent by $2N \times 2N$ complex matrices. They satisfy

$$J = \Sigma_N J^T \Sigma_N, \quad P_N^{(\text{AII}^\dagger)}(J) = C_N e^{-\text{Tr}(JJ^\dagger)}, \quad (\text{A7})$$

with Gaussian distribution of elements, normalization $C_N^{-1} = (\pi/2)^{2N^2-N}$, and Σ_N the skew-Hermitian metric,

$$\Sigma_N = \begin{pmatrix} 0 & -i\mathbb{1}_{N \times N} \\ i\mathbb{1}_{N \times N} & 0 \end{pmatrix}. \quad (\text{A8})$$

The NN and NNN spacing distributions have to be determined numerically again and are shown in Fig. 14 as histograms.

Also shown is a fit of the two respective spacing distributions to β in the 2dCG. The corresponding Kolmogorov-Smirnov distances (d) and standard deviations (σ) are given in Table VI, with best fits marked as bold numbers. For the

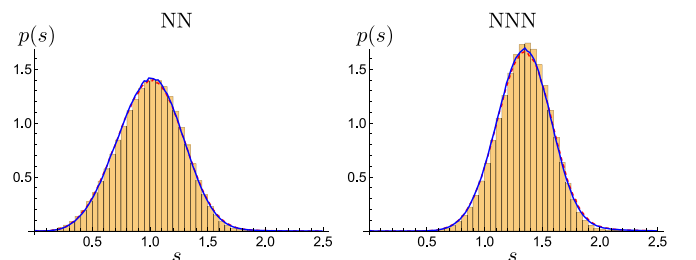


FIG. 14. Comparison of the NN (left) and NNN (right) spacing distribution for 500 matrices of size $2N = 5000$ of the symmetry class AII^\dagger (histogram), with the best fit of the 2dCG data for $\beta = 2.5$ (red dashed curve) and $\beta = 2.6$ (blue curve). The comparison to NNN is new here.

NN, the value $\beta = 2.6$ is slightly favored, which was also reported in [46]. For NNN, $\beta = 2.6$ again gives the best fit according to the standard deviations, whereas $\beta = 2.5$ is best for the Kolmogorov-Smirnov distance. This also shows that the next-to-nearest-neighbor spacing of the 2dCG with its

locally logarithmic repulsion gives a consistent approximation of this random matrix symmetry class AII^\dagger .

For comparison with the quality of fits in class A, where we have analytical predictions, we independently ran numerical simulations with matrices of the same size; see Table V.

-
- [1] M. V. Berry and M. Tabor, Level clustering in the regular spectrum, *Proc. R. Soc. London, Ser. A: Math. Phys. Sci.* **356**, 375 (1977).
 - [2] O. Bohigas, M.-J. Giannoni, and C. Schmit, Characterization of chaotic quantum spectra and universality of level fluctuation laws, *Phys. Rev. Lett.* **52**, 1 (1984).
 - [3] G. Casati, F. Valz-Gris, and I. Guarneri, On the connection between quantization of nonintegrable systems and statistical theory of spectra, *Lett. Nuovo Cim.* **28**, 279 (1980).
 - [4] L. D'Alessio, Y. Kafri, A. Polkovnikov, and M. Rigol, From quantum chaos and eigenstate thermalization to statistical mechanics and thermodynamics, *Adv. Phys.* **65**, 239 (2016).
 - [5] S. Müller, S. Heusler, P. Braun, F. Haake, and A. Altland, Semi-classical foundation of universality in quantum chaos, *Phys. Rev. Lett.* **93**, 014103 (2004).
 - [6] F. Haake, *Quantum Signatures of Chaos* (Springer, New York, 2010).
 - [7] W. Buijsman, V. Cheianov, and V. Gritsev, Random matrix ensemble for the level statistics of many-body localization, *Phys. Rev. Lett.* **122**, 180601 (2019).
 - [8] F. Minganti, A. Miranowicz, R. W. Chhajlany, and F. Nori, Quantum exceptional points of non-Hermitian Hamiltonians and Liouvillians: The effects of quantum jumps, *Phys. Rev. A* **100**, 062131 (2019).
 - [9] M. Naghiloo, M. Abbasi, Y. N. Joglekar, and K. W. Murch, Quantum state tomography across the exceptional point in a single dissipative qubit, *Nat. Phys.* **15**, 1232 (2019).
 - [10] F. Roccati, G. M. Palma, F. Ciccarello, and F. Bagarello, Non-Hermitian physics and master equations, *Open Syst. Inf. Dyn.* **29**, 2250004 (2022).
 - [11] R. Grobe, F. Haake, and H.-J. Sommers, Quantum distinction of regular and chaotic dissipative motion, *Phys. Rev. Lett.* **61**, 1899 (1988).
 - [12] H. Sompolinsky, A. Crisanti, and H.-J. Sommers, Chaos in random neural networks, *Phys. Rev. Lett.* **61**, 259 (1988).
 - [13] J. Ginibre, Statistical ensembles of complex, quaternion, and real matrices, *J. Math. Phys.* **6**, 440 (1965).
 - [14] R. Hamazaki, K. Kawabata, N. Kura, and M. Ueda, Universality classes of non-Hermitian random matrices, *Phys. Rev. Res.* **2**, 023286 (2020).
 - [15] D. Bernard and A. LeClair, A Classification of non-Hermitian random matrices, *Statistical Field Theories*, edited by A. Cappelli and G. Mussardo (Springer, New York, 2002), Vol. 73, pp. 207–214.
 - [16] U. Magnea, Random matrices beyond the Cartan classification, *J. Phys. A: Math. Theor.* **41**, 045203 (2008).
 - [17] N. Hatano and D. R. Nelson, Localization transitions in non-Hermitian quantum mechanics, *Phys. Rev. Lett.* **77**, 570 (1996).
 - [18] H. Markum, R. Pullirsch, and T. Wettig, Non-Hermitian random matrix theory and lattice QCD with chemical potential, *Phys. Rev. Lett.* **83**, 484 (1999).
 - [19] T. Kanazawa and T. Wettig, New universality classes of the non-Hermitian Dirac operator in QCD-like theories, *Phys. Rev. D* **104**, 014509 (2021).
 - [20] B. Ye, L. Qiu, X. Wang, and T. Guhr, Spectral statistics in directed complex networks and universality of the Ginibre ensemble, *Commun. Nonlinear Sci. Numer. Simul.* **20**, 1026 (2015).
 - [21] G. Akemann, M. Kieburg, A. Mielke, and T. Prosen, Universal signature from integrability to chaos in dissipative open quantum systems, *Phys. Rev. Lett.* **123**, 254101 (2019).
 - [22] A. Rubio-García, R. A. Molina, and J. Dukelsky, From integrability to chaos in quantum Liouvillians, *SciPost Phys. Core* **5**, 026 (2022).
 - [23] A. B. Jaiswal, A. Pandey, and R. Prakash, Universality classes of quantum chaotic dissipative systems, *Europhys. Lett.* **127**, 30004 (2019).
 - [24] Y. Huang and B. I. Shklovskii, Anderson transition in three-dimensional systems with non-Hermitian disorder, *Phys. Rev. B* **101**, 014204 (2020).
 - [25] G. Akemann, N. Chakarov, O. Krüger, A. Mielke, M. Ottensmann, and P. Päsler, Interactions between different birds of prey as a random point process, *J. Stat. Mech.* (2024) 053501.
 - [26] D. Basko, I. Aleiner, and B. Altshuler, Metal-insulator transition in a weakly interacting many-electron system with localized single-particle states, *Ann. Phys.* **321**, 1126 (2006).
 - [27] V. Oganesyan and D. A. Huse, Localization of interacting fermions at high temperature, *Phys. Rev. B* **75**, 155111 (2007).
 - [28] M. Žnidarič, T. Prosen, and P. Prelovšek, Many-body localization in the Heisenberg XXZ magnet in a random field, *Phys. Rev. B* **77**, 064426 (2008).
 - [29] A. Pal and D. A. Huse, Many-body localization phase transition, *Phys. Rev. B* **82**, 174411 (2010).
 - [30] J. H. Bardarson, F. Pollmann, and J. E. Moore, Unbounded growth of entanglement in models of many-body localization, *Phys. Rev. Lett.* **109**, 017202 (2012).
 - [31] A. D. Luca and A. Scardicchio, Ergodicity breaking in a model showing many-body localization, *Europhys. Lett.* **101**, 37003 (2013).
 - [32] D. A. Abanin, E. Altman, I. Bloch, and M. Serbyn, Colloquium: Many-body localization, thermalization, and entanglement, *Rev. Mod. Phys.* **91**, 021001 (2019).
 - [33] P. Sierant, M. Lewenstein, A. Scardicchio, L. Vidmar, and J. Zakrzewski, Many-Body localization in the age of classical computing, *Rep. Prog. Phys.* (2024).
 - [34] J. M. Deutsch, Quantum statistical mechanics in a closed system, *Phys. Rev. A* **43**, 2046 (1991).

- [35] M. Srednicki, Chaos and quantum thermalization, *Phys. Rev. E* **50**, 888 (1994).
- [36] M. Serbyn, Z. Papić, and D. A. Abanin, Local conservation laws and the structure of the many-body localized states, *Phys. Rev. Lett.* **111**, 127201 (2013).
- [37] V. Ros, M. Müller, and A. Scardicchio, Integrals of motion in the many-body localized phase, *Nucl. Phys. B* **891**, 420 (2015).
- [38] J. Z. Imbrie, Diagonalization and many-body localization for a disordered quantum spin chain, *Phys. Rev. Lett.* **117**, 027201 (2016).
- [39] R. Hamazaki, K. Kawabata, and M. Ueda, Non-Hermitian many-body localization, *Phys. Rev. Lett.* **123**, 090603 (2019).
- [40] L.-J. Zhai, S. Yin, and G.-Y. Huang, Many-body localization in a non-Hermitian quasiperiodic system, *Phys. Rev. B* **102**, 064206 (2020).
- [41] K. Suthar, Y.-C. Wang, Y.-P. Huang, H. H. Jen, and J.-S. You, Non-Hermitian many-body localization with open boundaries, *Phys. Rev. B* **106**, 064208 (2022).
- [42] S. Ghosh, S. Gupta, and M. Kulkarni, Spectral properties of disordered interacting non-Hermitian systems, *Phys. Rev. B* **106**, 134202 (2022).
- [43] G. De Tomasi and I. M. Khaymovich, Stable many-body localization under random continuous measurements in the no-click limit, *Phys. Rev. B* **109**, 174205 (2024).
- [44] F. Roccati, F. Balducci, R. Shir, and A. Chenu, Diagnosing non-Hermitian many-body localization and quantum chaos via singular value decomposition, *Phys. Rev. B* **109**, L140201 (2024).
- [45] S. Lapp, J. Ang'ong'a, F. A. An, and B. Gadway, Engineering tunable local loss in a synthetic lattice of momentum states, *New J. Phys.* **21**, 045006 (2019).
- [46] G. Akemann, A. Mielke, and P. Pöbller, Spacing distribution in the two-dimensional Coulomb gas: Surmise and symmetry classes of non-Hermitian random matrices at noninteger β , *Phys. Rev. E* **106**, 014146 (2022).
- [47] L. Sá, P. Ribeiro, and T. Prosen, Complex spacing ratios: A signature of dissipative quantum chaos, *Phys. Rev. X* **10**, 021019 (2020).
- [48] C. N. Yang and C. P. Yang, One-dimensional chain of anisotropic spin-spin interactions. I. Proof of Bethe's hypothesis for ground state in a finite system, *Phys. Rev.* **150**, 321 (1966).
- [49] D. E. Mahoney and J. Richter, Transport and integrability-breaking in non-Hermitian many-body quantum systems, *Phys. Rev. B* **110**, 134302 (2024).
- [50] K. Joel, D. Kollmar, and L. F. Santos, An introduction to the spectrum, symmetries, and dynamics of spin-1/2 Heisenberg chains, *Am. J. Phys.* **81**, 450 (2013).
- [51] W. Pauli, On Dirac's new method of field quantization, *Rev. Mod. Phys.* **15**, 175 (1943).
- [52] J. Feinberg and M. Znojil, Which metrics are consistent with a given pseudo-Hermitian matrix? *J. Math. Phys.* **63**, 013505 (2022).
- [53] A. Melkani, Degeneracies and symmetry breaking in pseudo-Hermitian matrices, *Phys. Rev. Res.* **5**, 023035 (2023).
- [54] This is after removing the term proportional to the identity, which is responsible for the constant imaginary shift in the complex plane.
- [55] We found that for $1d$, $\Sigma = 1.8\bar{s}$ gives good results.
- [56] D. Kundu, S. Kumar, and S. S. Gupta, Beyond nearest-neighbour universality of spectral fluctuations in quantum chaotic and complex many-body systems, [arXiv:2408.04345](https://arxiv.org/abs/2408.04345).
- [57] J. Li, S. Yan, T. Prosen, and A. Chan, Spectral form factor in chaotic, localized, and integrable open quantum many-body systems, [arXiv:2405.01641](https://arxiv.org/abs/2405.01641).
- [58] Such point may not be unique, but the event of finding two neighboring points at the very same distance will be of measure zero.
- [59] It is expected based on numerical simulations that the spacing distribution at the edge is different.
- [60] The effect of this rescaling on the logarithmic term amounts to adding a constant $(\beta/2) \ln \sqrt{2/\beta}$, which, in turn, becomes a multiplicative factor, $\exp[\frac{\beta N(N-1)}{4} \ln \sqrt{\beta/2}]$, in the joint distribution. In the limit $\beta \rightarrow 0$, this factor goes to 1.
- [61] For $N = 2$, the NN spacing distribution is known for classes AI^\dagger and AII^\dagger [14,23], which are, however, not a good approximation for the large- N limit, as was discussed in [46].
- [62] Equations (23) and (27) of Ref. [46] contain typos; we write down the corrected formula in (7).
- [63] M. L. Mehta, *Random Matrices* (Elsevier, Amsterdam, 2004).
- [64] P. J. Forrester, *Log-gases and Random Matrices (LMS-34)* (Princeton University Press, Princeton, NJ, 2010).
- [65] A. Borodin and C. D. Sinclair, The Ginibre ensemble of real random matrices and its scaling limits, *Commun. Math. Phys.* **291**, 177 (2009).
- [66] J. Sakhr and J. M. Nieminen, Wigner surmises and the two-dimensional homogeneous poisson point process, *Phys. Rev. E* **73**, 047202 (2006).
- [67] H.-J. Sommers, Y. V. Fyodorov, and M. Titov, S-matrix poles for chaotic quantum systems as eigenvalues of complex symmetric random matrices: From isolated to overlapping resonances, *J. Phys. A: Math. Gen.* **32**, L77 (1999).
- [68] T. Guhr, A. Müller-Groeling, and H. A. Weidenmüller, Random-matrix theories in quantum physics: Common concepts, *Phys. Rep.* **299**, 189 (1998).
- [69] A. M. García-García, L. Sá, and J. J. M. Verbaarschot, Universality and its limits in non-Hermitian many-body quantum chaos using the Sachdev-Ye-Kitaev model, *Phys. Rev. D* **107**, 066007 (2023).
- [70] In [21] it was suggested that $\alpha = 4.5$ is a good choice and we use this value too.
- [71] Y. Y. Atas, E. Bogomolny, O. Giraud, and G. Roux, Distribution of the ratio of consecutive level spacings in random matrix ensembles, *Phys. Rev. Lett.* **110**, 084101 (2013).
- [72] I. G. Dusa and T. Wettig, Approximation formula for complex spacing ratios in the Ginibre ensemble, *Phys. Rev. E* **105**, 044144 (2022).
- [73] It appears from numerics that classes AI^\dagger and AII^\dagger also have a flat spectrum in the bulk and thus do not require unfolding.
- [74] R. Grobe and F. Haake, Universality of cubic-level repulsion for dissipative quantum chaos, *Phys. Rev. Lett.* **62**, 2893 (1989).
- [75] G. Akemann, M. Phillips, and L. Shiffrin, Gap probabilities in non-Hermitian random matrix theory, *J. Math. Phys.* **50**, 063504 (2009).